

# Water Resources Research

## RESEARCH ARTICLE

10.1029/2020WR028771

### Special Section:

The Arctic: An AGU Joint  
Special Collection

### Key Points:

- Subsurface aqueous contaminant transport in permafrost regions is controlled by coupled water, energy, and reactive solute transport
- We developed a groundwater model to simulate reactive solute transport in permafrost landscapes
- Constitutive relationships describing solute-dependent freezing and temperature-dependent reaction rates strongly influence contaminant migration

### Supporting Information:

Supporting Information may be found in the online version of this article.

### Correspondence to:

V. F. Bense,  
[victor.bense@wur.nl](mailto:victor.bense@wur.nl)





### Citation:

Mohammed, A. A., Bense, V. F., Kurylyk, B. L., Jamieson, R. C., Johnston, L. H., & Jackson, A. J. (2021). Modeling reactive solute transport in permafrost-affected groundwater systems. *Water Resources Research*, 57, e2020WR028771. <https://doi.org/10.1029/2020WR028771>

Received 9 SEP 2020

Accepted 21 JUN 2021

## Modeling Reactive Solute Transport in Permafrost-Affected Groundwater Systems

Aaron A. Mohammed<sup>1</sup> , Victor F. Bense<sup>2</sup> , Barret L. Kurylyk<sup>1</sup> , Rob C. Jamieson<sup>1</sup> ,  
Lindsay H. Johnston<sup>1</sup>, and Amy J. Jackson<sup>1</sup>

<sup>1</sup>Department of Civil and Resource Engineering and Centre for Water Resources Studies, Dalhousie University, Halifax, NS, Canada, <sup>2</sup>Department of Environmental Sciences, Wageningen University and Research, Wageningen, The Netherlands

**Abstract** Understanding the interactions between ground freeze-thaw, groundwater flow, and solute transport is imperative for evaluating the fate of contaminants in permafrost regions. However, predicting solute migration in permafrost-affected groundwater systems is challenging due to the inherent interactions and coupling between subsurface mass and energy transport processes. To this end, we developed a numerical model that considers coupled groundwater flow, subsurface heat transfer, and solute transport, including water-ice phase change, solute-dependent porewater freezing, and temperature-dependent solute reaction rates. As an illustrative example, we present simulations to investigate the potential for contamination from a municipal wastewater lagoon in the Canadian sub-arctic. Two-dimensional groundwater models assuming varying permafrost conditions were developed to evaluate possible contaminant migration scenarios associated with groundwater flow from the lagoon to a river, including the transport of conservative, degradable, and sorbing solutes. Model results reveal important transport mechanisms controlling the behavior of aqueous contaminants in permafrost landscapes as well as the hydrogeologic factors affecting reactive transport in cold regions. Seasonal freeze-thaw episodically restricts connectivity of transport pathways, which attenuates both transport and reaction rates. However, elevated solute concentrations can depress the freezing temperature of porewater and produce thaw-induced solute transport. Both thermally driven and solute-enhanced thaw can decrease ice content in permafrost, which can have significant implications for solute migration. Therefore, thermo-hydrogeologic process controlling reactive transport in cold-region groundwater systems must be considered when quantitatively assessing the impact of changing environmental conditions on contaminant hydrogeology.

**Plain Language Summary** Groundwater contamination associated with increased human and industrial activity is a growing risk in northern regions. However, current groundwater flow models generally do not simulate both permafrost dynamics and reactive solute transport. In this study we develop a hydrological model to simulate groundwater flow and dissolved contaminant transport for permafrost environments. The new model was applied at a site in the Canadian sub-arctic to investigate the possibility of groundwater contamination associated with a wastewater lagoon. Results identified important mechanisms controlling the migration of contaminants in permafrost landscapes, including the effects of seasonal ground freezing and groundwater flow. Results show that the physical relationships describing the effects of contaminant levels on ground freezing characteristics and the influence of temperature on contaminant degradation properties strongly affect contamination movement. The new model will be useful for understanding how climate change and permafrost thaw will impact groundwater flow and associated subsurface migration of dissolved chemicals in cold regions.

## 1. Introduction

With increasing development in northern regions comes the growing risk for present-day groundwater contamination (Macdonald et al., 2005; McKenzie et al., 2021; Poland et al., 2003), and ongoing permafrost thaw due to climate change may release previously sequestered chemical species (Vonk et al., 2019). Many communities in the Arctic and subarctic utilize landfills and wastewater lagoons that are not underlain by engineered seepage barrier materials (Al-Houri et al., 2009; Daley et al., 2018; McCarter et al., 2017), possibly under the assumption that these are underlain by sufficiently impermeable frozen ground. With

© 2021. The Authors.

This is an open access article under the terms of the [Creative Commons Attribution-NonCommercial License](https://creativecommons.org/licenses/by-nc/4.0/), which permits use, distribution and reproduction in any medium, provided the original work is properly cited and is not used for commercial purposes.

surface warming, the possibility exists for dissolved solutes from these facilities to leach into groundwater and groundwater-fed waterways, potentially posing a risk to ecosystem health, and into drinking water supply relying on surface water (Burkow & Kallenborn, 2000; Hayward et al., 2018; Krumhansl et al., 2015; Macdonald et al., 2000). Considerable effort is required to identify, delineate, and remediate subsurface contamination. The use of groundwater flow and transport models to support management efforts is common practice; however, to address the potential for groundwater contamination in cold regions there is a need to adapt solute transport descriptions in mathematical models to account for the presence of pore ice and freezing temperatures (Panday & Corapcioglu, 1994; Vonk et al., 2019). Present solute transport models generally do not consider permafrost dynamics, while cold-regions groundwater models including solute transport routines are rare (Grenier et al., 2018; Lamontagne-Hallé et al., 2020). Previous research on subsurface contaminant transport in cold regions has predominantly focused on petroleum spills and active-layer transport of other non-aqueous phase liquids (Carlson & Barnes, 2011; Dyke, 2001; Panday & Corapcioglu, 1994). Few studies have focused on the behavior of aqueous solutes within active-layer and permafrost groundwater systems on relatively small spatial scales (Bosson et al., 2013; Frampton & Destouni, 2015; Yi et al., 2021). Consequently, there is a need to improve understanding of how changing permafrost conditions may impact groundwater flow and reactive solute transport dynamics in cold regions.

Although saturated ice-rich permafrost has a very strongly reduced permeability (up to seven orders of magnitude) compared to when liquid water occupies pore space, perennial taliks and active layer groundwater flow during seasonally unfrozen periods provide pathways for advective and dispersive contaminant migration above and below permafrost (Bosson et al., 2013; Johansson et al., 2015) as well as diffusion into permafrost containing unfrozen pore water (Barnes & Chuvilin, 2009; Biggar et al., 1998). Seasonal freeze-thaw and associated weathering processes can also enhance active-layer hydraulic conductivity and increase solute advection and dispersion (Ding et al., 2019; Koch et al., 2013; Mohammed et al., 2021). Additionally, the degradation and transformation of reactive solutes are driven by temperature-dependent biogeochemical activity and freezing conditions that mediate the fate of reactive solutes (Dusek et al., 2019; McCarter et al., 2017; Yurova et al., 2008). Improved conceptual and mathematical descriptions of coupled groundwater flow and reactive solute transport processes specific to cold regions are thus necessary to assess potential contamination in permafrost groundwater systems (McKenzie et al., 2021). Such model development is also needed for investigating changing groundwater-facilitated transport dynamics brought on by climate change and permafrost thaw (Bense et al., 2009; Frampton et al., 2013; Ge et al., 2011; Kurylyk et al., 2016; Walvoord et al., 2012), such as the transport of nutrients and heavy metals released from thawing permafrost soils (Neilson et al., 2018; Selroos et al., 2019; Vonk et al., 2019).

In this study, we developed a numerical cryohydrogeological model that considers groundwater flow, pore-water freeze-thaw, and reactive solute transport using physics-based descriptions of subsurface water, heat, and chemical transport, including constitutive relationships for water-ice phase change, sorption, and temperature-dependent solute degradation. The new model will be useful for studying how permafrost conditions impact groundwater flow and reactive solute transport for different contaminants across a range of geologic, hydrologic, and climatic conditions. As an illustrative example, we apply the model here in the first instance to investigate potential groundwater contamination associated with a wastewater lagoon facility in the Canadian subarctic. These simulations identified important transport mechanisms controlling the behavior of conservative, sorbing, and degrading aqueous contaminants in permafrost regions. Results are interpreted to support site investigations to assess the possible impacts of the wastewater lagoon on nearby groundwater and surface water quality.

## 2. Model Development

The generic finite-element modeling environment FlexPDE (PDE Solutions Inc., 2020, <http://www.pdesolutions.com>) was used to solve the partial differential equations and constitutive relationships describing coupled groundwater flow, reactive solute transport, and heat transfer with freeze-thaw. Cryohydrogeological models built within FlexPDE have been previously validated against benchmarked numerical solutions of groundwater flow and permafrost thaw (Grenier et al., 2018) and applied to permafrost groundwater systems without solute transport (Bense et al., 2009, 2012). This section describes the water, heat and reactive transport equations used in this study.

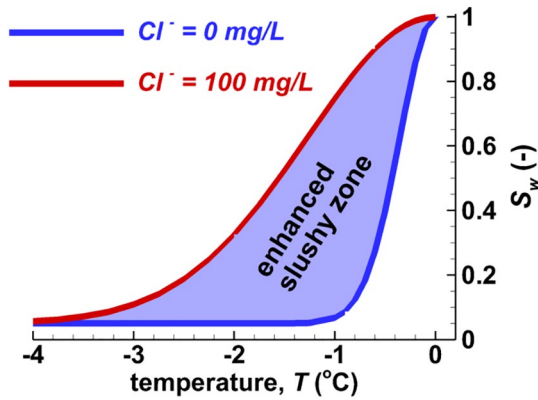


**Figure 1.** Modified soil freezing characteristic used in this study for simulations S1b and S2b. The purple region shows the increase in liquid water saturation between 0 to  $-3.5^{\circ}\text{C}$  with elevated chloride concentrations up to  $100\text{ mg L}^{-1}$ .

Assuming saturated subsurface conditions, water flow is described by (Bense et al., 2009):

$$\frac{\rho_w g}{\mu} \nabla \cdot [k_{rw} k \nabla h] = S_s \frac{\partial h}{\partial t} \quad (1)$$

where,  $h$  [m] is the hydraulic head,  $\rho_w$  [ $\text{kg m}^{-3}$ ] is fluid density,  $g$  [ $\text{m s}^{-2}$ ] is acceleration due to gravity,  $\mu$  [ $\text{kg m}^{-1} \text{s}^{-1}$ ] is dynamic viscosity of water,  $k$  [ $\text{m}^2$ ] is the intrinsic permeability of porous medium,  $k_{rw}$  [-] is a relative permeability exponential function that reduces permeability as pore ice is formed (McKenzie et al., 2007), and  $S_s$  [ $\text{m}^{-1}$ ] is the porous medium specific storage. Energy transport and subsurface temperatures ( $T$  [ $^{\circ}\text{C}$ ]) are modeled using the conduction-advection equation considering the effects of latent heat associated with the melting/freezing of pore ice:

$$\nabla \cdot [\kappa_e \nabla T] - C_w \nabla \bar{q} T = C_a \frac{\partial T}{\partial t} + L_i \frac{\partial \theta_w}{\partial t} \quad (2)$$

where  $\kappa_e$  [ $\text{W m}^{-1} \text{K}^{-1}$ ] and  $C_a$  [ $\text{J m}^{-3} \text{K}^{-1}$ ] are respectively the effective thermal conductivity and volumetric heat capacity of the sediment/fluid/ice mixture,  $\theta_w$  [ $\text{m}^3 \text{m}^{-3}$ ] is the liquid water content, and  $\bar{q}$  [ $\text{m s}^{-1}$ ] is the Darcy flux ( $k_{rw} k \nabla h$ ), i.e., groundwater flow in Equation 1 drives advective heat transport.  $C_w$  [ $\text{J m}^{-3} \text{K}^{-1}$ ] and  $L_i$  [ $\text{J m}^{-3}$ ] are the volumetric water heat capacity and volumetric latent heat of fusion, respectively. The reduction in effective liquid water saturation,  $S_w$  [-] as temperatures decrease and ice forms is described using an empirical exponential function approximation of the soil freezing curve (SFC) (Lunardini, 1988; McKenzie et al., 2007):

$$S_w = (1 - S_{wres}) e^{-(T/W)^2} + S_{wres} \quad (3)$$

where  $S_{wres}$  [-] is the residual liquid saturation and  $W$  (K) is an empirical parameter related to the temperature transition window over which liquid water decreases from saturation to  $S_{wres}$  as ice forms (Lunardini, 1988).

Experimental evidence has shown that certain soluble salts (e.g., Chloride ( $\text{Cl}^-$ )) decrease the freezing temperature of porewater by increasing the osmotic potential of the aqueous solution in the porous medium (Cary & Mayland, 1972; Ginot et al., 2020). The net effect of this phenomenon on the SFC is to increase the amount of liquid water present at sub-zero temperatures and increase the temperature window of the water-ice transition period or the “slushy zone” of the SFC (Ginot et al., 2020). In this study, solutes are not expected to significantly affect porewater freezing beyond this effect (as maximum measured  $\text{Cl}^-$  concentrations in the lagoon were approximately  $100\text{ mg L}^{-1}$ , and seawater  $\text{Cl}^-$  concentration is around  $19,400\text{ mg L}^{-1}$  for reference). Thus, here we employed a simple modification to the SFC to consider the effects of concentration-dependent freezing as follows. First, the SFC for groundwater with a  $\text{Cl}^-$  concentration of  $100\text{ mg L}^{-1}$  was approximated using the salinity-dependent SFC formulation by Zhou et al. (2020). The curve fitting parameter  $W$  in Equation 3 was then adjusted to approximately match the change in SFC (Figure 1). Thus for  $\text{Cl}^-$  solute transport,  $W$  is linearly increased from 0.5 to 1.8 over the solute concentration range of 0– $100\text{ mg L}^{-1}$  (Figure 1). This formulation enables us to represent the effect of elevated  $\text{Cl}^-$  concentrations on the liquid water present and thus the permeability for temperatures from 0 to  $-3.5^{\circ}\text{C}$  (Biggar et al., 1998; Panday & Corapcioglu, 1994). Expressions for all constitutive relations and parameters values used in Equations 1–3 are listed in Table 1.

In addition to the mediating effects of pore ice on advective-dispersive transport and concentration-dependent porewater freezing, the reactivity of solutes in groundwater involves temperature-dependent degradation processes such as microbially driven mineralization and biodegradation, and physio-chemical processes such as adsorption/desorption (Fan et al., 2010). To make the model numerically tractable when coupling solute transport to both water flow and heat transfer, simplifying assumptions had to be made. (a) The effects of solute concentration on fluid density were not considered (see above discussion of lagoon

**Table 1**

*Physical Parameter Values and Expressions Used in the Water and Heat Transport Equations*

Physical properties	Units	Values or expressions
porosity, $n$	$\text{m}^3 \text{m}^{-3}$	0.4
Aquifer compressibility, $\beta$	$\text{m s}^2 \text{kg}^{-1}$	$1.0 \times 10^{-8}$ (includes both water and matrix)
Gravitational acceleration, $g$	$\text{m s}^{-2}$	9.81
Aquifer specific storage, $S_s$	$\text{m}^{-1}$	$S_s = n\beta S_w \rho_w g$ (Bense et al., 2009)
Thermal conductivity of water, $\kappa_w$	$\text{W m}^{-1} \text{K}^{-1}$	0.6
Thermal conductivity of ice, $\kappa_i$	$\text{W m}^{-1} \text{K}^{-1}$	2.14
Thermal conductivity of solids, $\kappa_s$	$\text{W m}^{-1} \text{K}^{-1}$	3.5
Effective thermal conductivity, $\kappa_e$	$\text{W m}^{-1} \text{K}^{-1}$	$\kappa_e = nS_w \kappa_w + n(1 - S_w) \kappa_i + (1 - n) \kappa_s$
Specific heat of water, $c_w$	$\text{J kg}^{-1} \text{K}^{-1}$	4,182
Specific heat of ice, $c_i$	$\text{J kg}^{-1} \text{K}^{-1}$	2,060
Specific heat of solid grains, $c_s$	$\text{J kg}^{-1} \text{K}^{-1}$	835
Water density, $\rho_w$	$\text{kg m}^{-3}$	1,000
Ice density, $\rho_i$	$\text{kg m}^{-3}$	920
Solid grain density, $\rho_s$	$\text{kg m}^{-3}$	2,650
Dynamic viscosity of water, $\mu$	$\text{kg m}^{-1} \text{s}^{-1}$	$1.3 \times 10^{-3}$
Bulk volumetric heat capacity, $C_a$	$\text{J m}^{-3} \text{K}^{-1}$	$C_a = nS_w \rho_w c_w + n(1 - S_w) \rho_i c_i + (1 - n) \rho_s c_s$
Volumetric latent heat of fusion for water, $L_i$	$\text{J m}^{-3}$	Ice density $\times$ mass-based latent heat = $3.03 \times 10^8$ (Bense et al., 2009)
Residual saturation, $S_{wres}$	–	0.05
$W$	K	0.5 (“clean” water) to 1.8 (“dirty” water)
Liquid water content, $\theta_w$	$\text{m}^3 \text{m}^{-3}$	$\theta_w = n S_w$
Hydraulic conductivity, $K_w$	$\text{m s}^{-1}$	$K_w = k_{rw} k \rho_w g / \mu$
Intrinsic permeability, $k$	$\text{m}^2$	$1.4 \times 10^{-12}$ – $1.4 \times 10^{-17}$ (See Figure 2)
Relative permeability, $k_{rw}$	–	$k_{rw} = 10^{-\Omega(1-S_w)^n}$ (McKenzie et al., 2007)
Impedance factor, $\Omega$	–	50

$\text{Cl}^-$  concentrations). (b) An equilibrium approach was used to describe solute sorption (Dusek et al., 2019). (c) First-order kinetics were assumed for solute degradation (Yurova et al., 2008). Solute reaction processes include sorption and degradation as mass sources or sinks in addition to advective-dispersive transport:

$$\nabla \cdot [\mathbf{D} \nabla C] - \nabla v_i C - \lambda_a C = \frac{\partial C}{\partial t} + \frac{\rho_b}{n} \frac{\partial S_C}{\partial t} \quad (4)$$

where  $C$  [ $\text{mg L}^{-1}$ ] is the solute concentration,  $\mathbf{D}$  [ $\text{m}^2 \text{s}^{-1}$ ] is the hydrodynamic dispersion tensor defining solute spreading by mechanical dispersion and molecular diffusion whose terms have been modified for the presence of pore ice (Table 2),  $v_i$  [ $\text{m s}^{-1}$ ] is the linear fluid velocity ( $v_i = \bar{q}/\theta_w$ ) accounting for the presence of pore ice (Table 2), with the groundwater velocity from the flow equation (Equation 1) driving the advective solute flux. Terms  $\rho_b$  [ $\text{kg m}^{-3}$ ] and  $n$  [ $\text{m}^3 \text{m}^{-3}$ ] are the bulk density and porosity of the porous medium, and  $S_C$  [ $\text{g kg}^{-1}$ ] is the adsorbed concentration of solutes onto the aquifer matrix. Solute reactions are coupled to heat transport through the degradation term,  $\lambda_a$  [ $\text{s}^{-1}$ ], which is the temperature-dependent first-order coefficient for solute degradation. The temperature dependency and associated coupling to heat transport in the degradation term is described using a modified Van't Hoff equation describing the exponential increase in the rate of biological activity with temperature (Yurova et al., 2008):

**Table 2**  
Parameter Values and Expressions Used in the Solute Transport Equation

Physical properties	Units	Values or expressions
Horizontal dispersion component, $D_{xx}$	$\text{m}^2 \text{s}^{-1}$	$D_{xx} = \alpha_L v_x^2 /  v  + \alpha_T v_y^2 /  v  + D_m$ (Bear, 1972)
Vertical dispersion component, $D_{yy}$	$\text{m}^2 \text{s}^{-1}$	$D_{yy} = \alpha_L v_y^2 /  v  + \alpha_T v_x^2 /  v  + D_m$ (Bear, 1972)
Diagonal dispersion components, $D_{xy}, D_{yx}$	$\text{m}^2 \text{s}^{-1}$	$D_{xy} = D_{yx} = (\alpha_L - \alpha_T) v_x v_y /  v $ (Bear, 1972)
Longitudinal dispersivity, $\alpha_L$	m	10
Transverse dispersivity, $\alpha_T$	m	1
Linear fluid velocity, $v_i$	$\text{m s}^{-1}$	$v_i = \bar{q} / \theta_w$ (Cary & Mayland, 1972)
Molecular diffusion coefficient, $D_m$	$\text{m}^2 \text{s}^{-1}$	$D_m = D_m^{\text{ref}} S_w^3$ (Cary & Mayland, 1972)
Reference molecular diffusion coefficient, $D_m^{\text{ref}}$	$\text{m}^2 \text{s}^{-1}$	$1.0 \times 10^{-9}$
Factor for increase in metabolic rate per 10 °C increase in temperature, $Q_{10}$	–	1.7 (Yurova et al., 2008)
Reference temperature, $T_{\text{ref}}$	°C	5.0
Reference degradation coefficient for N, $\lambda_a^{\text{ref}}$	$\text{s}^{-1}$	$1.91 \times 10^{-7}$ (Wittgren & Mrehlum, 1997)
Adsorbed solute concentration, $S_C$	$\text{g kg}^{-1}$	$S_C = K_D C$ (Dusek et al., 2019)
Sorption distribution coefficient for total P, $K_D$	$\text{m}^3 \text{kg}^{-1}$	$1.5 \times 10^{-2}$ (McCray et al., 2005)
Aquifer matrix bulk density, $\rho_b$	$\text{kg m}^{-3}$	1,250
Initial concentration for conservative solute	$\text{mg L}^{-1}$	100
Initial concentration for total N (degrading)	$\text{mg L}^{-1}$	80
Initial concentration for total P (sorbing)	$\text{mg L}^{-1}$	10

$$\lambda_a = \lambda_a^{\text{ref}} \cdot Q_{10}^{0.1(T - T_{\text{ref}})} \quad (5)$$

where  $\lambda_a^{\text{ref}}$  is the reference degradation rate for the reference temperature,  $T_{\text{ref}}$  [°C], and  $Q_{10}$  is the factor for increase in metabolic rate per 10 °C increase in temperature. Sorption,  $S_C$  (Table 2) is modeled assuming a linear equilibrium sorption approach (Dusek et al., 2019). The implementation of Equation 4 in FlexPDE was benchmarked against the classic Ogata and Banks (1961) analytical solution, and Equations 1–3 have been extensively benchmarked in Grenier et al. (2018). Equations 1, 2 and 4 are solved simultaneously so that solute, heat, and groundwater transport are coupled using constitutive relations in Tables 1 and 2. Expressions for all relations and values for all parameters used in Equations 4 and 5 are listed in Table 2.

### 3. Illustrative Model Application

Our new model was applied to investigate the potential for groundwater contamination associated with a wastewater lagoon facility in the Northwest Territories, Canada (Figure 2). For this site, models of groundwater flow, subsurface heat transfer, and reactive solute transport were developed and parameterized based on measured data including local climate, vegetation cover, soil and sediment properties, topography, groundwater depths, and seasonal air temperature variations. However, the lack of permafrost and active layer thickness data at this stage, along with the high probability of thawing permafrost in the area, precluded the ability to do a thorough data-model comparison or calibration (e.g., Albers et al., 2020). Thus, the specific objective of this modeling exercise was to evaluate the potential for subsurface solute migration associated with groundwater flow from the lagoon to reach the river for a range of conditions. Simulations were run for different scenarios of initial permafrost distributions (i.e., surface temperature conditions) to generate a range of possible contamination transport pathways associated with the water flow into the aquifer from



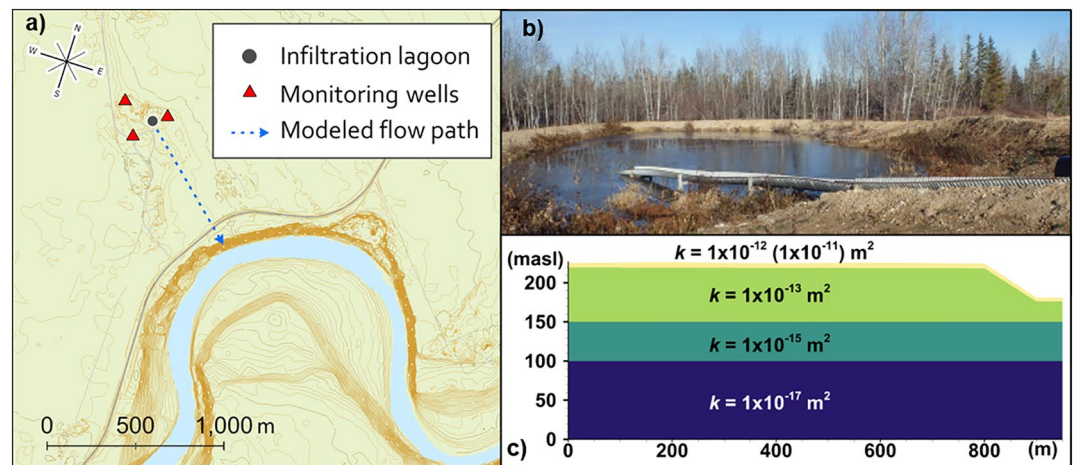


**Figure 2.** (a) Plan view of study site showing the location of the lagoon and monitoring wells as well as the transect used for simulations; (b) a picture of the lagoon taken in October 2018; and (c) model domain showing permeability distribution used in simulations: scenarios S3b and S4b use an upper layer (upper 5 m, yellow layer) permeability of  $1 \times 10^{-11} \text{ m}^2$ , and all other scenarios use an upper layer permeability of  $1 \times 10^{-12} \text{ m}^2$ .

the lagoon and its impact on the development of a contaminant plume in the underlying groundwater and its potential to exfiltrate into nearby surface water.

### 3.1. Field Site

The hydrogeological system underlying a wastewater lagoon (Figure 2a), is located near a small rural community in northern Canada, with a population of approximately 110 people. The exact location of the community cannot be specified due to confidentiality reasons. The lagoon (Figure 2b) is located approximately 900 m northwest of a river in the region. The region has an average annual precipitation of 336 mm, with average winter air temperatures of  $-22^\circ\text{C}$  in January and  $+16^\circ\text{C}$  in July (Government of Canada, 2019), with an average annual air temperature of  $-2^\circ\text{C}$ . However, permafrost in the region, where present, is relatively warm and generally closer to  $-1^\circ\text{C}$  (Smith et al., 2009). The site is located in the subarctic zone of discontinuous permafrost (Heginbottom & Radburn, 1992; Smith et al., 2009), and is expected to be underlain by permafrost to some degree. As is the regional trend, the subsurface at the site is likely warming, triggering permafrost thaw. Currently, the active-layer groundwater flow season has a duration of approximately 4–5 months, from May to September/October, but is possibly year-long where permafrost has already degraded substantially and a supra-permafrost aquifer has developed.

The lagoon is approximately 30 m in diameter and 2 m deep. The lagoon water surface is consistently 1–2 m below the ground surface and is connected to the local water table (Figure 2b). The lagoon is surrounded by a mixture of trees and forested areas and marshy/wetland areas, indicating shallow/local groundwater discharge areas within 500 of the lagoon. Municipal wastewater is delivered to the lagoon daily. Site investigations in 2016 show that the topography of the site slopes toward the southeast, draining toward the river (Figure 2). Lateral hydraulic gradients measured via monitoring wells (installed to a depth of 6 m below ground surface) in the vicinity of the lagoon (Figure 2a) were on average approximately 0.01 m/m, and indicated groundwater flows east toward the river. For the purposes of this modeling investigation, the shortest flow path to the river (Figure 2a), was assumed to be the dominant groundwater flow direction to simulate a worst-case contamination scenario for the river. Borehole logs and soil/sediment surveys generally classified the geology at the site as glacial till consisting of sandy gravel or sandy clay underlain by clay-rich till. Slug tests in monitoring wells indicated that hydraulic conductivities in the upper sandy gravel and sandy clay units where permafrost is absent ranged from  $10^{-4}$  to  $10^{-6} \text{ m s}^{-1}$  respectively. Field investigations also identified several water quality parameters (e.g., ammonia-nitrogen, chloride) that were above background concentrations in the monitoring wells (Figure 2), indicating the contaminating impact of the exfiltration lagoon on local groundwater.

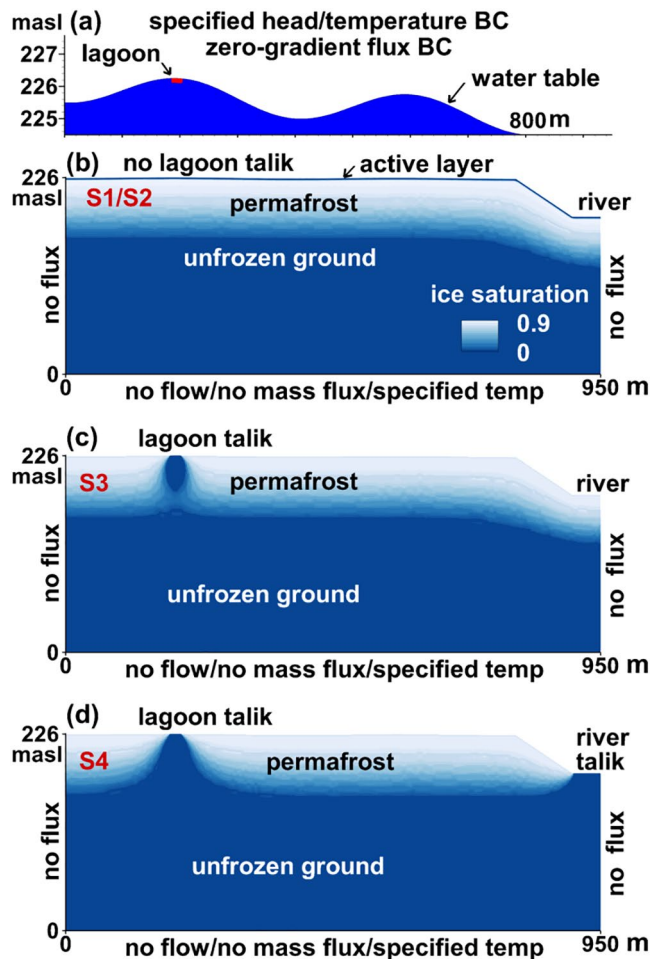


**Figure 3.** Model domain; initial and boundary conditions for (a) lagoon and water table at  $x = 0-800$  m for all scenarios (zoomed in and vertically exaggerated), (b) entire domain with permafrost conditions for scenarios S1 and S2 with no taliks present, (c) entire domain with permafrost conditions for scenario S3 with a talik underneath the lagoon, (d) entire domain with permafrost conditions for scenario S4 with taliks underneath both the lagoon and river.

water table is relatively shallow at the lagoon facility, it was assumed to follow surface topography. Hydraulic head along the top of the domain was fixed to represent a water table boundary condition (Figure 3a). Consequently, recharge occurred at the ridge of the hillslope, and regional discharge was focused in the topographic low adjacent to the river (Figure 3d). The base and vertical sides of the model were “no-flow” hydraulic boundaries to represent catchment divides (Figure 3b). For heat transport, a uniform temperature of  $2^{\circ}\text{C}$  was assigned to the base of the domain (i.e., below the permafrost base) rather than a geothermal heat flux (Ge et al., 2011) to form permafrost from the top-down, while the vertical sides were closed for heat exchange (Figure 3b). The upper specified temperature boundary condition varied according to the simulation scenario (discussed below). Initial conditions shown for groundwater flow and permafrost conditions (Figure 3) were developed by running the model to a dynamic equilibrium condition (simulated for 1,000 years) with an average annual temperature of  $-1^{\circ}\text{C}$  (or  $-2^{\circ}\text{C}$  for one scenario discussed below) applied to the top of the domain to generate permafrost. The generation and impact of taliks are discussed below. As FlexPDE employs time-step control and dynamic adaptive mesh refinement, element size and vertical discretization ranged from 0.01 to 10 m during simulations, with finer mesh discretization needed in the active layer and permafrost.

### 3.2. Groundwater Modeling Strategy

#### 3.2.1. Permafrost and Active-Layer Properties

The cyro-hydrogeological model developed here can incorporate spatiotemporal distributions of hydrothermal properties in multiple dimensions, but is currently limited to two-dimensional mass and energy transport in the saturated subsurface for numerical tractability. Thus, estimates of ground and near-surface temperatures are needed to provide upper thermal boundary conditions (Evans et al., 2020; Kurylyk et al., 2016; Langford et al., 2020). Permafrost and active-layer depths are governed by subsurface heat transfer, which is driven mainly by thermal conduction between the ground surface and underlying subsurface (Hayashi et al., 2007; Sjöberg et al., 2016). Ground surface temperatures are determined by the surface energy balance of heat fluxes due to radiation, sensible heat, latent heat (i.e., evaporation, condensation), and ground conduction (Hinzman et al., 1998).

To make use of available meteorological data and account for these factors, the surface energy balance of the site was initially simulated using a one-dimensional soil-vegetation-atmosphere-transfer model which accounts for ground freeze-thaw conditions. The SHAW model (Flerchinger & Saxton, 1989; Mohammed et al., 2017) was used to estimate the expected ground temperatures and active-layer and permafrost-table depths. The initial estimates of ground temperatures and active-layer depths from the SHAW simulations were used to inform the range of surface thermal boundary conditions employed in the groundwater model. These were then combined with available site geology, topography and groundwater information to develop the domain and boundary conditions for the groundwater model. Information regarding the SHAW simulations can be found in the Supporting Information.

#### 3.2.2. Model Domain, Initial Conditions, and Boundary Conditions

The groundwater model domain employed represents a two-dimensional topography-driven groundwater flow system underlain by permafrost. Topography at the lagoon site slopes gently toward the river to the southeast (Figure 3). A 2 m-resolution digital elevation map of the site was used to extract the surface topography along a 2-D transect that represented the minimum distance between the lagoon and the river (Figure 2a). As the

To simulate contaminant transport associated with lagoon effluent, a specified concentration boundary condition for the contaminant of interest was applied along a portion of the water table under the lagoon (Figure 3a). For other regions along the top boundary, a boundary condition was specified such that any recharging water had a concentration of  $0 \text{ mg L}^{-1}$ . The concentration of water exiting the domain, that is, groundwater discharge, was determined by the simulated advective solute flux leaving the model, representing the possible contaminant loading to the river. The base and sides of the model were closed to mass fluxes (Figure 3). The model initially had no contaminant mass present in the system. Three contaminants were simulated: (a) a conservative solute; (b) total nitrogen, a degrading solute; and (c) total phosphorus, a sorbing solute.

### 3.2.3. Model Scenarios

Five simulation scenarios are presented as illustrative examples of possible permafrost, groundwater flow, and solute transport conditions (Table 3). For the first simulation scenario, referred to as S1, the top domain temperature boundary condition was specified such that the seasonally maximum active-layer depths were  $\sim 2\text{--}2.5 \text{ m}$  in the groundwater model. The temperature along the top boundary was prescribed using a sinusoidal seasonal temperature cycle with a mean of  $-1^\circ\text{C}$  and amplitude of  $8^\circ\text{C}$  to force a seasonal active layer and drive episodic shallow active-layer groundwater flow (Figures 3b and 3d). Simulations were run from initial conditions for 50 years without (S1a) and with (S1b) the modified concentration dependent SFC (Figure 1). Scenario S2 (S2a and S2b) were similar to S1 but had permafrost generated from an average surface temperature of  $-2^\circ\text{C}$ . A seasonal signal with a mean of  $-2^\circ\text{C}$  and amplitude of  $8^\circ\text{C}$  was then applied to generate colder and, therefore, thicker permafrost and thinner active layer conditions.

Simulations S3 and S4 were run with continuous surface warming (thawing permafrost) and the presence of taliks with no modification to the SFC. S3 has a talik present under the lagoon, generated by increasing the initial average surface temperature over the lagoon from  $-1^\circ\text{C}$  to  $5^\circ\text{C}$ . S4 has taliks under both the lagoon and river, with the lagoon talik generated in the same manner as S3 and the river talik generated by applying an average surface temperature of  $2^\circ\text{C}$  over the river. The difference in lagoon talik configuration between S3 (closed talik in Figure 3c) and S4 (open talik in Figure 3d) is due to the presence of the river talik which increases the hydraulic connection between the lagoon and river. The implications of this connection are discussed later in the results section. These simulations were subjected to a constant linear surface warming signal of  $0.05^\circ\text{C}/\text{year}$  for 100 years (consistent with warming scenario RCP 8.5 (Collins et al., 2013)) from their initial condition.

Scenario S5 represented a highly idealized model domain with flow restricted to a thin, shallow aquifer and no seasonal freezing or permafrost present to maximize the rate of contaminant transport and examine the “worst-case” scenario for contaminant loading to the river. Scenarios S1 to S5 were designed to evaluate the possible range of permafrost conditions and the effect on contaminant loading to the river (Table 3). Simulation scenarios S1 and S2 were run for 50 years, S3 and S4 for 100 years, and S5 for 500 years. Specified concentrations applied to the lagoon boundary conditions (Table 2) were based on water samples taken from the lagoon. The parameters for contaminant degradation and sorption were estimated based on available literature for similar processes and/or systems, and the temperature dependency in terms described in Section 2 (Dusek et al., 2019; Yurova et al., 2008). Values for all parameters are listed in Tables 1 and 2.

## 4. Results and Discussion

The model results presented in the following sections are discussed and interpreted to elucidate the complex interplay between coupled water, heat, and solute transport dynamics in permafrost-affected groundwater systems.

### 4.1. Effects of Permafrost Conditions on Groundwater Dynamics

Figure 4 illustrates the simulated hydraulic head and hydraulic conductivity distributions for scenarios S1–S4. In scenarios S1 and S2, during the active-layer flow period, the flow regime was shallow and flow rates near the lagoon (Figure 4a) were approximately  $10^{-7} \text{ m s}^{-1}$ . Reduced hydraulic conductivity of the



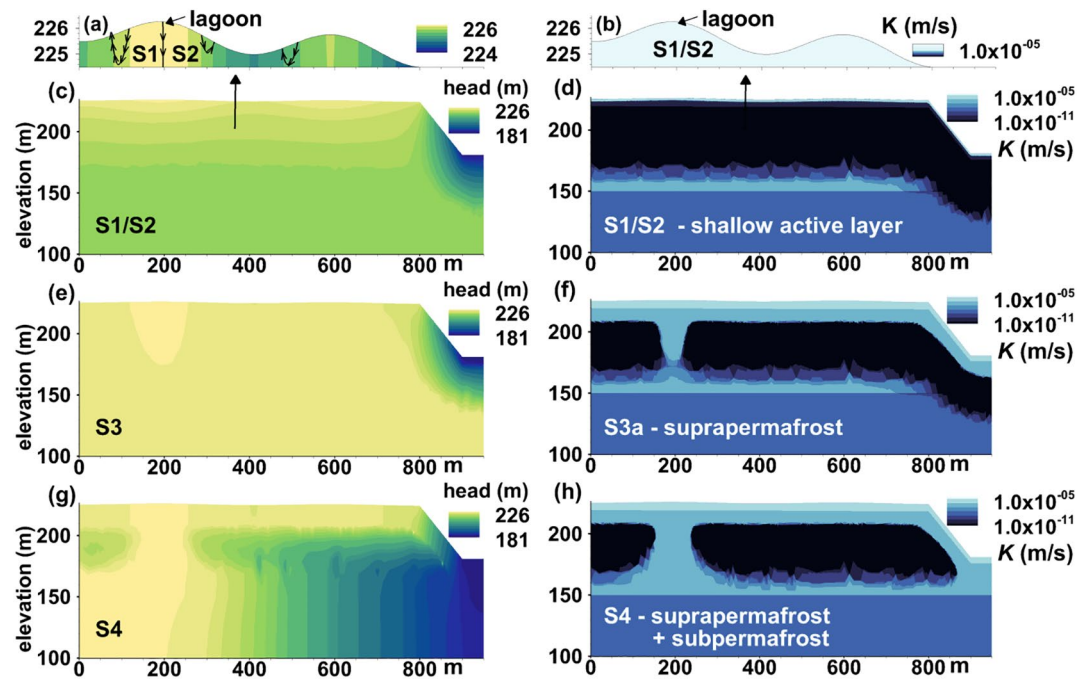


**Figure 4.** Left panel shows simulated hydraulic head distributions, and right panels show simulated hydraulic conductivity distributions accounting for the presence of pore ice for: (a and b) Scenarios S1 and S2 (active layer close-up during thawed period, note scale difference from panels below); (c and d) Scenarios S1 and S2 at  $t = 50$  years; (e and f) Scenario S3 at  $t = 100$  years; and (g and h) scenario S4 at  $t = 100$  years.

permafrost (Figures 4b and 4d) restricted flow and thus the potential transport of contaminants to the shallow active layer during unfrozen periods. Also, the surface topography generated shallow local flow reversals away from the regional gradient to the river (Figures 4a and 4c), which combined with the shallow flow system, seasonal freezing in the active layer, and stable permafrost at depth, limited transport from the lagoon directly to the river. Figure 5 shows the temperature distributions at the beginning and end of the simulations for all scenarios. For scenarios S1 and S2 (Figures 5a–5d), temperature conditions were stable and did not change during the simulation period.

Results from scenarios S3 and S4 show that the presence of taliks had a significant effect on groundwater flow dynamics (Figure 4), and thus, taliks are also expected to have a strong control on the spatial distribution of solutes from the lagoon. For S3 with a talik present only under the lagoon, essentially all flow was confined to the thawing active layer in the supra-permafrost flow system (Figure 4e), as the talik's hydraulic connectivity was limited vertically (Figure 4f); however, there was increased downward flow in the talik itself which increased temperatures below the lagoon (Figures 5e and 5f). In contrast, in scenario S4, with taliks beneath the lagoon and river, the downward flow enhanced both the hydraulic (Figures 4g and 4h) and thermal (Figures 5g and 5h) connections to the river, which vertically opened the lagoon talik compared to scenario S3 (Figures 4e and 4f) and facilitated sub-permafrost flow in addition to the supra-permafrost system.

The range of groundwater flow conditions in scenarios S1–S4 are significantly different, representing: (a) a shallow episodic active-layer flow system in S1 and S2; (b) a supra-permafrost flow system in S3; and (c) a combined supra-permafrost and sub-permafrost flow system in S4. These differing flow, thermal, and freeze-thaw regimes would thus be expected to exert a strong control on the maximum extent and distribution of solute mass present in the system.

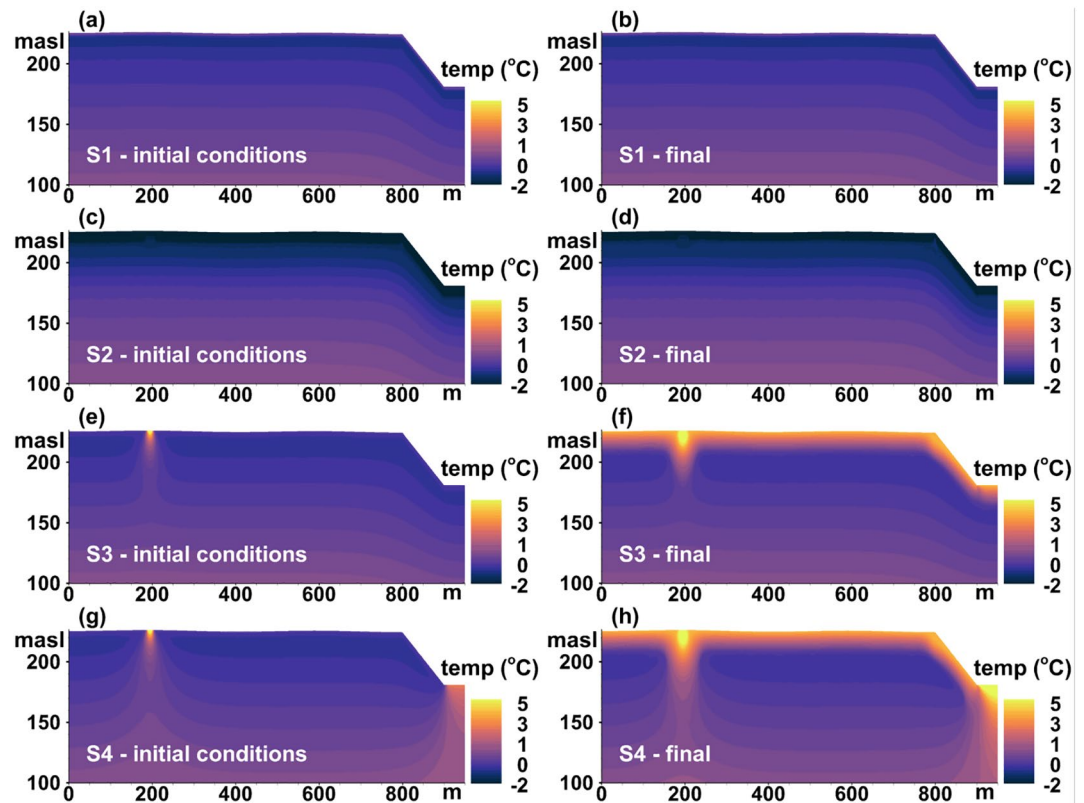


**Figure 5.** Initial (left) and final (right) temperature distributions for simulation scenarios. The left panels show initial conditions for: (a) scenario S1, (c) scenario S2, (e) scenario S3, and (g) scenario S4. The right panel shows final temperature distributions for: (b) scenarios S1 at  $t = 50$  years, (d) scenario S2 at  $t = 50$  years, (f) scenario S3 at  $t = 100$  years, and (h) scenario S4 at  $t = 100$  years.

#### 4.2. Contaminant Transport and Migration in Stable Permafrost

Contaminant plumes and permafrost conditions at the end of the 50-years simulation period of S1 (stable climate and seasonal active layer at an average surface temperature of  $-1^{\circ}\text{C}$ ) are shown in Figure 6, for plumes with the unmodified SFC (S1a, panels a–d), and for the concentration-dependent SFC (S1b, panels e–h). For scenario S1a, the conservative solute plume (Figure 6b), defined as the extent of the 10 mg/L iso-line, extended to approximately 5 m below the domain surface; however, the bulk of the mass was within the upper 2.5 m, coinciding with the maximum seasonal thaw-depth of the active layer. The plume migrated

**Table 3**  
Key Details and Differences in Simulation Scenarios

Simulation scenario	Active layer conditions	Avg. Surface temperature	Permafrost conditions	Upper 5 m layer $k$	SFC type
S1a	Seasonal active layer	$-1^{\circ}\text{C}$	Stable/no talik	$10^{-12} \text{ m}^2$	Thermal only
S1b	Seasonal active layer	$-1^{\circ}\text{C}$	Stable/no talik	$10^{-12} \text{ m}^2$	Thermal + solute-affected
S2a	Seasonal active layer	$-2^{\circ}\text{C}$	Stable/no talik	$10^{-12} \text{ m}^2$	Thermal only
S2b	Seasonal active layer	$-2^{\circ}\text{C}$	Stable/no talik	$10^{-12} \text{ m}^2$	Thermal + solute-affected
S3a	Thawing active layer	$-1^{\circ}\text{C}$	Thawing/lagoon talik	$10^{-12} \text{ m}^2$	Thermal only
S3b	Thawing active layer	$-1^{\circ}\text{C}$	Thawing/lagoon talik	$10^{-11} \text{ m}^2$	Thermal only
S4a	Thawing active layer	$-1^{\circ}\text{C}$	Thawing/lagoon + river talik	$10^{-12} \text{ m}^2$	Thermal only
S4b	Thawing active layer	$-1^{\circ}\text{C}$	Thawing/lagoon + river talik	$10^{-11} \text{ m}^2$	Thermal only
S5	No seasonal frost	$2^{\circ}\text{C}$	No permafrost	$10^{-12} \text{ m}^2$	No SFC

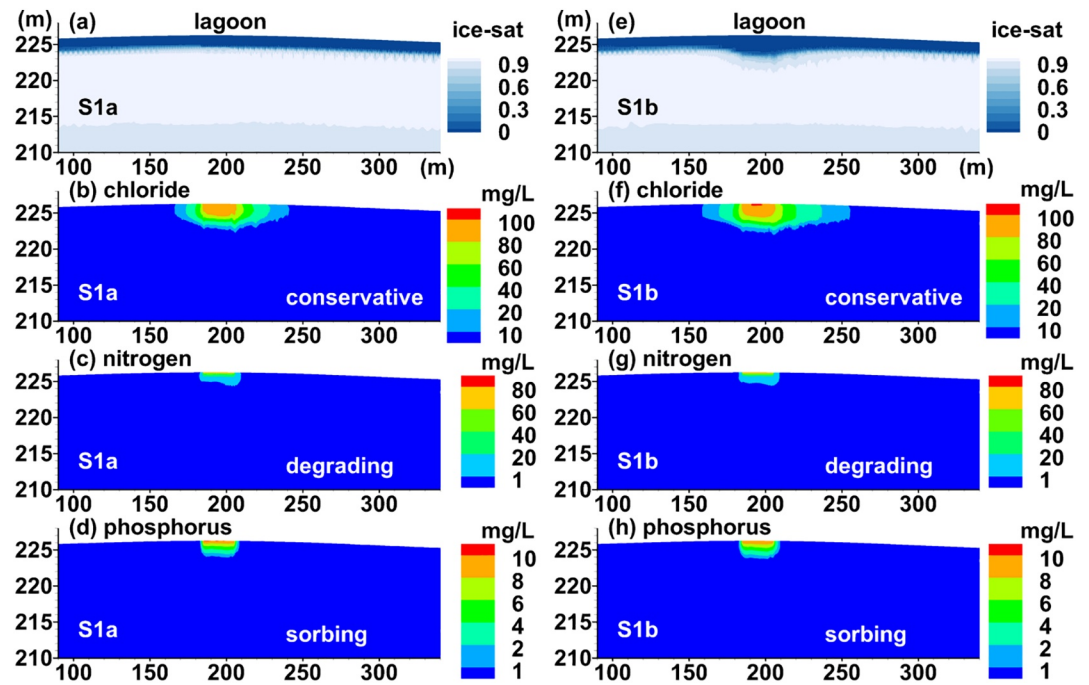


**Figure 6.** Results for S1a and S1b comparing simulations without (left) and with (right) the modified SFC with stable permafrost at an average temperature of  $-1^{\circ}\text{C}$ . Panels (a–d) show results of scenario S1a at simulated time = 50 years showing (a) ice-saturation at the maximum seasonal active layer thaw depth, and plumes for (b) chloride, (c) nitrogen, and (d) phosphorus. Panels (e–h) show results for scenario S1b (modified SFC) with (e) ice-saturation distribution at the maximum seasonal active layer thaw-depth where salt concentrations have decreased the ice-saturation around the lagoon, and plumes for (f) chloride, (g) nitrogen, and (h) phosphorus.

laterally approximately 50 m toward to the river, and about 30 m in the opposite direction due to local flow against the regional gradient that is toward the river, highlighting that regional groundwater movement in the region around the lagoon was limited by seasonal freezing in the active layer and relatively shallow flowpaths, as observed in earlier studies for other sites and settings (Lamontagne-Hallé et al., 2018; Sjöberg et al., 2016). The reactive nitrogen plume (Figure 6c), defined as the extent of the 1 mg/L isoline, was far less persistent due to degradation combined with temporary immobilization from seasonal freezing. In this case, the degradation rate rivaled the advective flux of the contaminant driven by groundwater flow, resulting in minimal horizontal migration ( $\sim 10$  m) of the reactive contaminant in these simulations. The phosphorus plume (Figure 6d), defined as the extent of the 1 mg/L isoline, was also less persistent than the conservative solute, as most mass was adsorbed during active-layer transport. Both nitrogen and phosphorus plumes range in depths from 2–3 m below the base of the lagoon, which was near the base of the active layer.

Simulations for scenario S1b (Figures 6e–6h), where  $\text{Cl}^-$  concentrations affect the SFC (Figure 1) show that elevated salt concentrations can potentially have an important effect on contaminant migration, even at levels far below that of seawater and neglecting variable density effects on buoyancy-driven flow components. All plumes showed enhanced migration relative to their corresponding simulations in S1a (Figure 6). In particular, the conservative salt and phosphorous plumes showed noticeable increases in mass transport due to solute-induced thaw (Figures 6g and 6h). For example, the largest lateral plume extent (chloride in Figure 6f) was increased by 27% for the scenario with a solute-dependent SFC compared to the scenario without (chloride in Figure 6b). This solute-induced thaw locally decreased pore ice around the lagoon which increased the effective permeability of the permafrost (Figure 6e) and allowed for further solute migration compared to S1a. The nitrogen plume, however, did not show an increase in mass compared to S1a (Figure 6g), as the degradation rate was still higher than the advective fluxes. These results show that when solutes allow more liquid water to be present at freezing temperatures, transport may be enhanced due to the increased permeability of permafrost as it becomes “slushy” near the thawing point (Ginot et al., 2020).

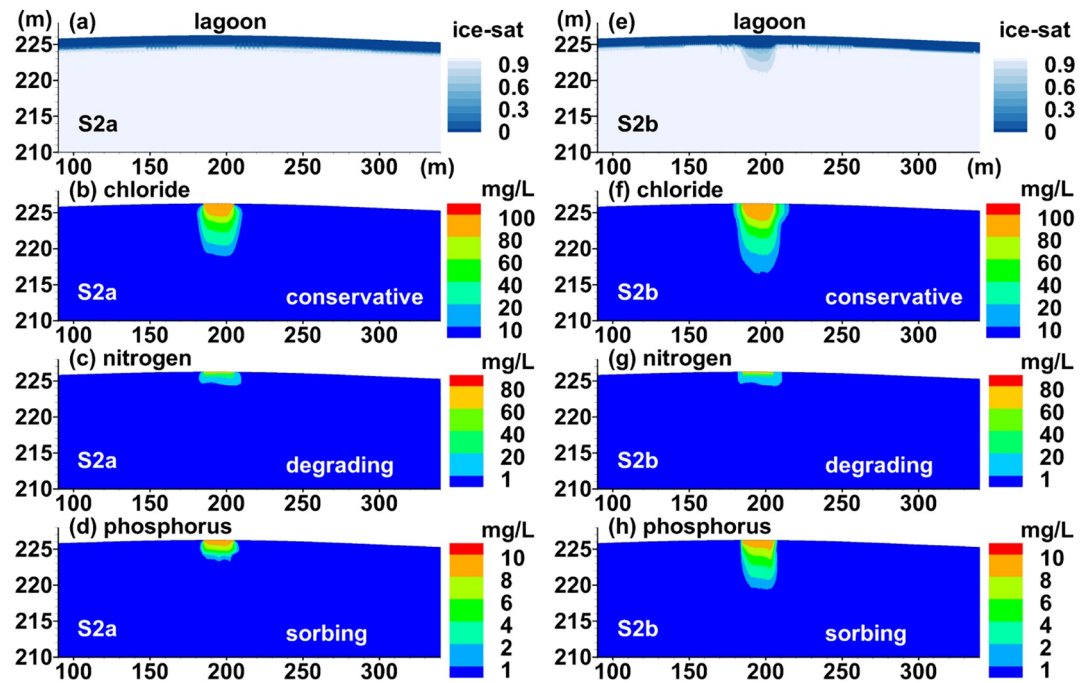


**Figure 7.** Results for S2a and b with stable permafrost at a surface temperature of  $-2^{\circ}\text{C}$ , that is, similar to S1 but under colder conditions. Panels (a–d) show results of scenario S2a at simulated time = 50 years showing (a) ice-saturation distribution at the maximum seasonal active layer thaw-depth, and plumes for (b) chloride, (c) nitrogen, and (d) phosphorus. Panels (e–h) show results for scenario S2b (modified SFC) with (e) ice-saturation distribution at the maximum seasonal active layer thaw-depth, and plumes for (f) chloride, (g) nitrogen, and (h) phosphorus.

Figure 7 shows results for scenarios S2a and S2b, which had colder permafrost due to the lower average surface temperature ( $-2^{\circ}\text{C}$ ). The maximum seasonal active layer thickness (Figure 7a) in these scenarios was approximately 2 m, which was only 0.5 m less than for S1 (Figure 6a). However, in scenario S2a, the chloride plume's horizontal extent (Figure 7b) was reduced by  $\sim 150\%$  compared to S1, but increased vertically by 40% ( $\sim 2$  m) (Figure 7b vs. Figure 6b). Less horizontal transport in this scenario increased the vertical concentration gradients around the lagoon causing more downward diffusion compared to S1a. The nitrogen plume (Figure 7c) did not show a similar increase, and was only slightly larger in extent than for S1a due to the degradation rate overpowering this increase in diffusion (Figure 6c). The phosphorus plume mass (Figure 7d) also only increased modestly with depth compared to S1a (Figure 6d), due to increased sorption.

For scenario S2b, with the solute-dependent SFC, the increase in vertical transport of chloride in S2 compared to S1, translated into a similar increase in solute-induced thaw (Figure 7e), and corresponding increase in chloride concentrations with depth (Figure 7f). The degrading nitrogen plume again did not change much compared to S2a or S1. However, the increase in solute-enhanced thaw caused the phosphorus plume extent (Figure 7h) to considerably increase with depth compared to S2a and both scenarios in S1, despite colder permafrost conditions. Figure 8 shows the difference in ice-saturation during the winter period when surface temperatures were at  $-1^{\circ}\text{C}$  (Figures 8a and 8b) and  $-2^{\circ}\text{C}$  (Figures 8c and 8d). These subtle differences in S1b and S2b in Figure 8 show that the influence of solute-enhanced thaw is less important for colder permafrost conditions, that is, it becomes less noticeable as temperatures decrease below the temperature-transition window of the SFC, but this can still have important implications for the migration of solutes (e.g., chloride and phosphorus in scenarios S1 and S2). From a modeling perspective, the simplified implementation of the concentration-dependent SFC limits the description of  $W$  in Equation 3 as an effective parameter that would need to be adjusted depending on the range of salinities present at the site being modeled. More physically based relationships between salinity and soil freezing (Zhou et al., 2020) would circumvent this. Another important numerical implication of these results is that if salt concentrations do affect the SFC, then multiple solutes need to be simultaneously simulated to produce the effect of increased liquid water content and consequent enhanced permeability on the migration of other solutes



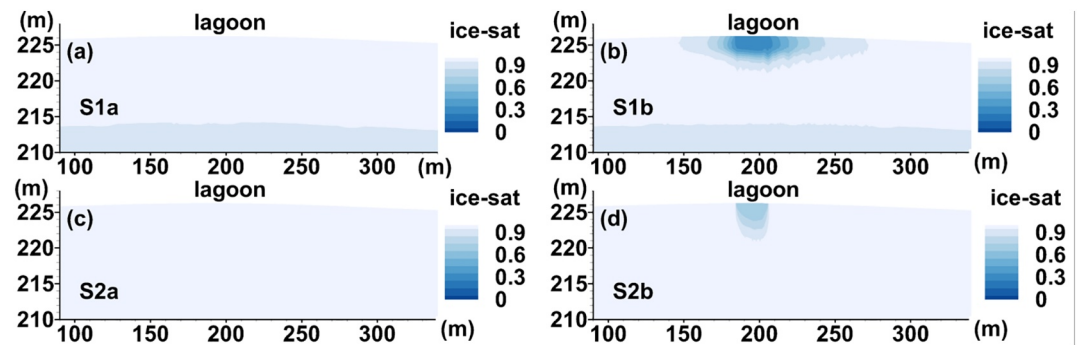


**Figure 8.** Top panels show the ice-saturation distribution when surface temperatures are at  $-1^{\circ}\text{C}$  during the seasonal temperature cycle for (a) S1a and (b) S1b. Lower panels show the ice-saturation distribution when surface temperatures are at  $-2^{\circ}\text{C}$  (colder conditions) during the seasonal temperature cycle for (c) S2a and (d) S2b. Differences in ice saturation between the left and right panels are due to the new modified SFC, highlighting that the difference salt concentrations have an effect on ice-saturation in permafrost.

present in the system. S1b and S2b were ran with all three species being simulated in parallel, which significantly increased run times.

#### 4.3. Contaminant Transport in Thawing Permafrost

Scenarios S3a and S4a were run from a stable initial condition (surface temperature =  $-1^{\circ}\text{C}$ ) and forward modeled subject to a constant surface warming of  $0.05^{\circ}\text{C}/\text{year}$  so that thaw continuously occurred (Figures 5g and 5h). At the end of 100 years in S3a, with a closed talik under the lagoon, the conservative plume was pooled at the base of the thawed layer with little diffusion of solute mass into the ice-rich permafrost (Figures 9a and 9b). Horizontally, the plume migrated approximately 225 m down gradient of the lagoon and 190 m upgradient of it. Compared to scenarios S1 and S2 with stable permafrost and shallow episodic groundwater flow (Figures 6 and 7), the conservative solute plume extent was greatly enhanced, and a much larger area around the lagoon was impacted. The solute mass from the lagoon however still did not reach the river in this simulation and was constrained at depth by the deepening permafrost table. It should be noted that nitrogen and phosphorus plumes were still much less persistent and are similar in extent to S1 and S2 despite the loss of permafrost.

In S4a, with an open talik underneath the lagoon, the conservative plume now extended through the talik to depths of 60 m below the surface of the domain (Figure 9f), but with the same horizontal extent as S3a. Again, similar to S3a, the degrading and sorbing plumes were less persistent despite permafrost loss (Figures 9g and 9h). These results, along with those of scenarios S1 and S2 suggest that permafrost, if present and stable, can be an effective barrier to contaminant migration from the lagoon. As expected, thawing permafrost allows for the enhanced migration of solutes (Connolly et al., 2020), and the presence of taliks enhances the depth of solute migration (Johansson et al., 2015). However, the model shows that solute transformation processes like sorption and degradation, can significantly reduce solute migration despite permafrost degradation and increased groundwater flow and subsurface hydrologic connectivity.

Solute migration results for scenarios S3b and S4b with a high permeability in the upper 5 m of the domain (Figure 2c; Table 3) are shown in Figure 10. The increased permeability of this layer resulted in much more groundwater flow and thus more solute mass present in the system for conservative solutes (Figures 10b and 10f) compared to the base case scenarios, but did not increased the plume's extent down gradient (Figures 9b and 9f). This was due to local groundwater discharge, consistent with the presence of wetlands and marshy areas at the field site (Section 3.1). The degrading nitrogen plumes are more persistent in these scenarios and extended approximately 150 m from the lagoon. In these scenarios, however, the conservative plumes still did not impact the river in the 100-year simulation period. It should be noted that the presence of a high permeability surficial layer in scenarios S3b and S4b (Figure 10) allowed the transport regime to become uncoupled from thaw dynamics, as the high conductivity kept most water flow within the near surface layer (upper 5 m), above the thawing permafrost table (Figures 10a and 10e). Scenarios S3 and S4



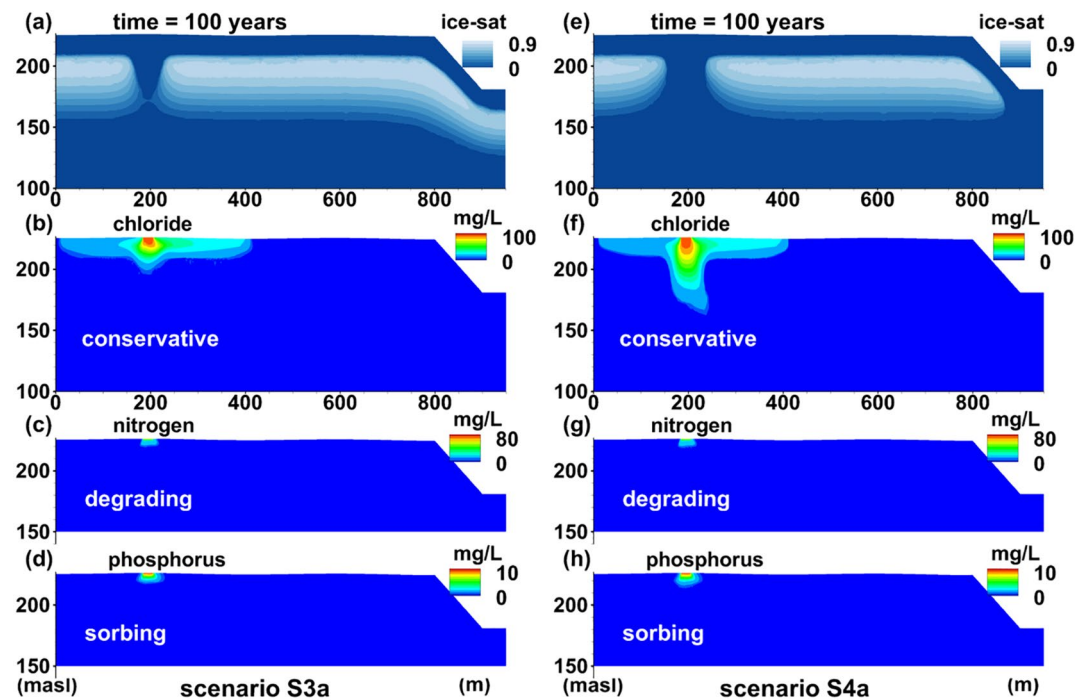


**Figure 9.** Results for S3a and S4a with surface warming and a talik under the lagoon only (S3a, left panels) and under both the lagoon and river (S4a, right panels). Panels (a–d) show results of scenario S3a at simulated time = 100 years showing (a) ice-saturation distribution, and plumes in (b) conservative solute, (c) total nitrogen, and (d) total phosphorus. Panels (e–h) show results for scenario S4a with (e) ice-saturation, and plumes for (f) conservative solute, (g) total nitrogen, (h) and total phosphorus.

highlight conditions under which permafrost presence is not the main driver of solute transport dynamics, and show that under certain conditions hydraulic (Figures 10b and 10f) and/or reaction properties (reactive plumes in Figures 9 and 10) may drive the fate and persistence of solutes rather than the presence of permafrost.

The S5 simulation scenario utilized a highly idealized model domain to purposefully impose hydrogeologic conditions that would maximize the rate of contaminant transport to the river. The model domain was reduced to 3 m in thickness to represent only the active layer, and no freeze-thaw was simulated so that the subsurface never froze and groundwater flow occurred year-long from the lagoon to the river. Under these conditions, breakthrough of the conservative solute at the river occurred at approximately 11 years (Figure 11a). For the degradable contaminant nitrogen, breakthrough never occurred (Figure 11b), and the plume reached a dynamic steady-state condition upgradient of the river. Figure 10c shows that the phosphorus (sorbing solute) plume migrated more than 600 m, but still had not reached the river after 500 years.

#### 4.4. Contamination Risk to River

Based on simulations conducted in these scenarios (Table 3), the likelihood of contaminants associated with the wastewater lagoon at the study site reaching the river is low. Simulations suggest groundwater and surface water in the immediate vicinity (~250 m) of the lagoon may be impacted by more conservative solutes (e.g., chloride). As the water table at the site is relatively close to surface where roots, fractures, and macropore networks exist, shallow preferential flow near the lagoon (which were not simulated) or thawing permafrost (which was simulated) may allow degradable solutes to affect this immediate vicinity as well. As the site is in a region of discontinuous permafrost with known permafrost degradation (Smith et al., 2009), results from scenarios S3 and S4 are more likely to represent reality at the field site. Evidence to support this include elevated concentration of solutes in the monitoring wells within 250 m of the lagoon (Supporting

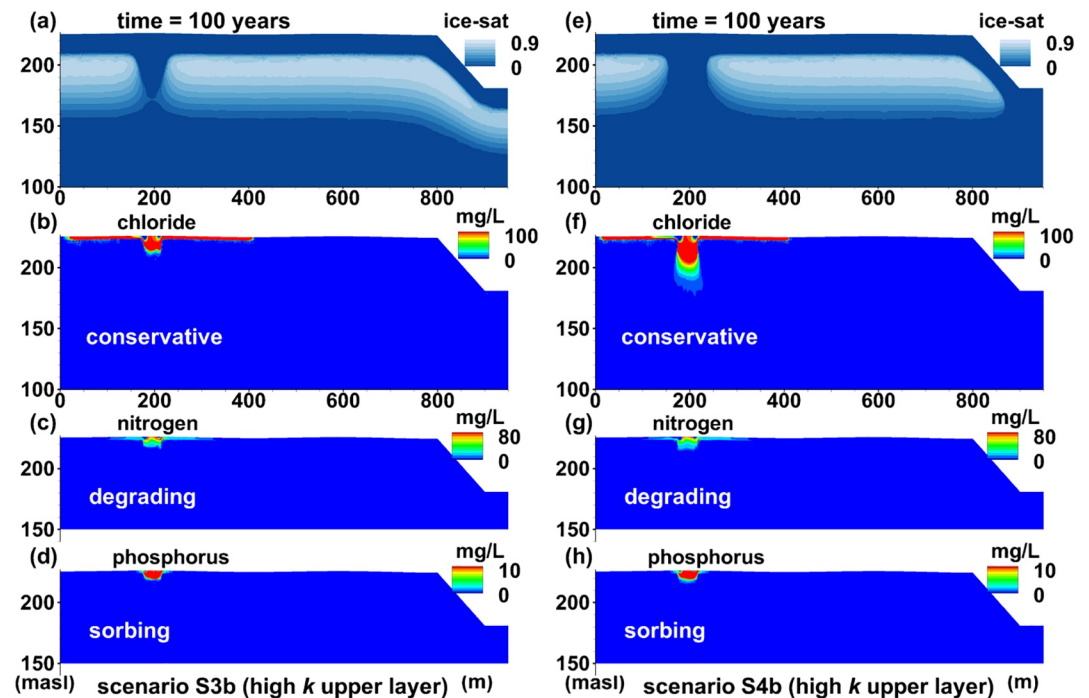


**Figure 10.** Results for scenarios S3b and S4b with a higher permeability upper layer and surface warming and a talik under the lagoon only (S3b) and under both the lagoon and river (S4b) at simulated time = 100 years. Panels (a–d) show results of scenario S3b at simulated time = 100 years showing (a) ice-saturation, and plumes in (b) conservative solute, (c) total nitrogen, and (d) total phosphorus. Panels (e–h) show results for scenario S4b with (e) ice-saturation, and plumes for (f) conservative solute, (g) total nitrogen, and (h) total phosphorus.

information S1). Areas of local groundwater discharge such as marshes and wetlands in the area may also be affected by persistent solutes (Figures 9 and 10).

It should be noted that the approach utilized here, in which only the saturated zone was modeled, does not consider the formation of a shallow perched aquifer and shallow subsurface flow which is the major runoff mechanism in many boreal forests in permafrost environments (Evans & Ge, 2017; Jafarov et al., 2018; Jan et al., 2020; Neilson et al., 2018). However, this pertains to snowmelt-driven runoff (surface and subsurface) and event flow generation, and not groundwater recharge to the permanently saturated zone and base-flow generation. Because the lagoon is located at a local topographic high, snowmelt from the surrounding landscape is unlikely to enter the lagoon, and thus neglecting this mechanism should not invalidate the main site-specific conclusions. However, we acknowledge the current model formulation and site conceptualization preclude consideration of these flow mechanisms, and future modeling should consider these processes to assess our assumptions.

Despite these limitations, all simulations, including “worst-case” scenarios, show that degradable solutes are likely naturally attenuated in this specific setting before discharge to the river. For example, in these simulations, nitrogen (degrading solute) or phosphorous (sorbing solute) plumes are unlikely to ever reach the river. This preliminary modeling suggests that if permafrost is present, this type of wastewater management approach could be a viable option for other similar small communities in the North. However, as scenarios here have shown, the performance of this type of system depends on a multitude of site-specific factors including topography, hydrogeology, soil properties, distance to surface water systems, climate, and permafrost (hydraulic and thermal) conditions. Also, systems that may perform well today may fail in the future due to climate change and concomitant permafrost thaw and activated groundwater flow systems.

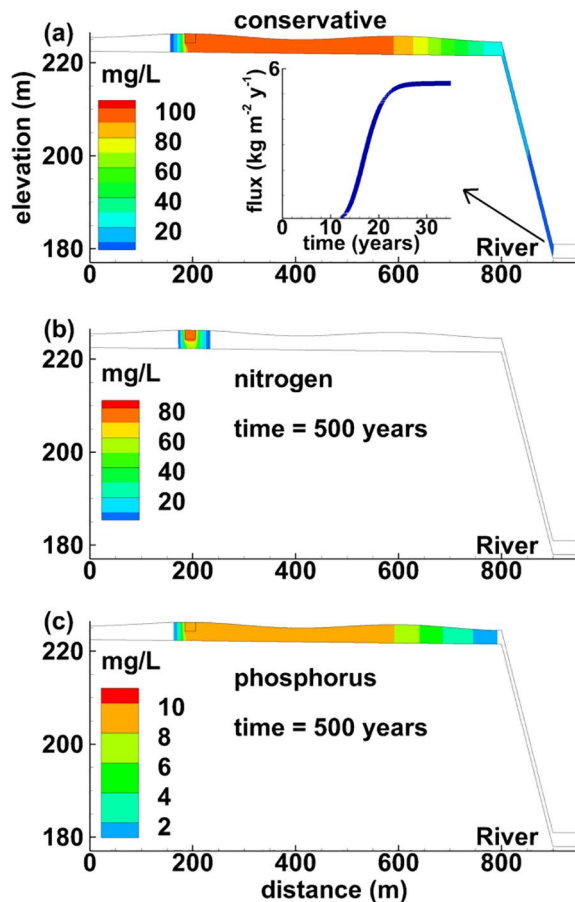


**Figure 11.** Scenario S5 simulation with no permafrost showing (a) conservative plume (10 mg/L isoline) reaching the river at approximately 11 years and breakthrough curve (inset); (b) total nitrogen (10 mg/L isoline) and (c) phosphorus (1 mg/L isoline) plumes at 500 years and never reaching the river. Note the nitrogen simulation reaches a dynamic steady state, whereas phosphorus was still migrating toward the river at 500 years.

#### 4.5. Model Limitations and Future Work

Key limitations of the model presented are: (a) it does not currently simulate vadose (unsaturated) zone processes; (b) it does not consider fluid density changes; and (c) it handles concentration-dependent freezing in a simplified manner that requires calibration. In addition to significantly reducing computational effort, these simplifications were considered acceptable in our example as the lagoon effluent concentrations were not expected to alter fluid density enough to affect results (e.g., the Raleigh stability criterion (Schincariol et al., 1997) was not exceeded). The addition of unsaturated zone flow and transport would allow for perched aquifer dynamics described above (Section 4.4) that were not represented here, and allow for more complex solute degradation and reaction processes to be accommodated in the model, such as thaw-induced mobilization of heavy metals and saturation-dependent organic matter decomposition from Arctic soils. Inclusion of variable-density flow and more physically based constitutive relations describing the effects of solutes on porewater freeze-thaw would enable the model to be applied to more diverse cold region environments such as coastal permafrost settings. Further research is underway to incorporate these processes and examine how they affect transport and reaction mechanisms in cold region hydrogeological systems. The difficulty of understanding the complex mechanisms governing contaminant/nutrient fate and transport in thawing permafrost environments necessitate more field and experimental data to validate emerging models like the one presented here.

There have already been significant advancements, albeit limited in number, in other methods of simulating solute transport and permafrost processes in groundwater models, such as particle tracking and Lagrangian travel-time based methods (Bosson et al., 2013; Frampton & Destouni, 2015). It should be noted that the simulations here neglected subsurface heterogeneities in flow, transport, and reaction properties, which travel-time methods have been able to efficiently capture, even with multi-component solute reaction and water-rock interaction processes (Cvetkovic et al., 2012; Malmström et al., 2004; Trinchero et al., 2020). The approach presented here which utilizes the advection-dispersion equation provides another useful tool for simulating reactive solute transport in permafrost groundwater systems. Furthermore,

the methodology employed here where constitutive relationships were used to couple heat and solute transport equations and relate solute reactivity to temperature conditions and heat transfer, cannot currently be simulated with a particle-tracking approach. This approach can also be incorporated into other similar formulations of groundwater flow and advective-dispersive mass/energy transport models (e.g., McKenzie et al., 2007; Diersch, 2013; Dagenais et al., 2020). It should be noted that the coupling of multiple transport equations in this approach, is computationally burdensome compared to particle tracking methods. However, massively parallelized multi-physics hydrological models like ATS (Painter et al., 2016), PFLOTRAN-ice (Karra et al., 2014), and OpenFoam (Orgogozo et al., 2019), have robust numerical schemes and already have multiple heat transfer, solute transport, and multiphase flow routines incorporated, and thus also have the numerical structure to accommodate the coupled heat-solute transport processes presented here.

#### 5. Summary and Conclusions

This study presented the development and application of a physically based numerical model for simulating solute transport in permafrost-affected groundwater systems. Simulations identified important coupled water-heat-solute transport mechanisms controlling the fate of groundwater contaminants in permafrost

regions, including how pore ice limits pore-connectivity and associated advective-dispersive transport. A modified concentration-dependent SFC showed that when elevated solute concentrations decrease the freezing temperature of porewater, thawed-induced transport can occur and may be an important process that facilitates the growth of contaminant plumes in warm permafrost. In addition, seasonal freezing causes the temporary immobilization of water and solutes, which increases solute residence times in the active layer. These mobilization-immobilization cycles combined with different degradation properties lead to species-specific transport times and mass attenuation dynamics, which strongly influence solute degradation processes. Shallow flow and seasonal freezing in the active layer restrict connectivity of flow and transport pathways to regional discharge zones. This creates longer transport pathways and increased residence times, solute reactions, and thus contaminant degradation.

As the climate warms and permafrost degrades, transport pathways and hydrologic connectivity increase due to enhanced deep groundwater flow through taliks and enhanced supra-permafrost groundwater flow, which expectedly increases the transport of conservative solutes. However, this also increases temperature-dependent solute reactions and sorption to unfrozen aquifer material, which makes the fate of reactive solutes dependent on other hydrogeologic factors in addition to permafrost presence/absence. Further model development should consider surface water and vadose zone processes, as well as more complex subsurface heterogeneities in flow and transport parameters. Incorporating more physically based descriptions of solute effects on porewater freezing should also be investigated. Finally, more field-based research is required to validate predictions from these new models, and to develop site assessment and science-based guidelines specifically for waste management facilities operating in subarctic and Arctic regions.

## Data Availability Statement

The SHAW model is publicly available free of charge at <https://www.ars.usda.gov/pacific-west-area/boise-id/northwest-watershed-research-center/docs/shaw-model/>. FlexPDE (version 7.19) is a commercial code that can be purchased and downloaded at <https://www.pdesolutions.com/>. FlexPDE scripts used in this study are available on a public repository (<https://data.mendeley.com/datasets/924kr89tfg/1>).

## Acknowledgments

The authors wish to thank Jeanne Arseneault and Rick Walbourne (Department of Environmental and Natural Resources, Government of Northwest Territories), Justin Hazenberg and Jamie Goddard (Municipal and Community Affairs, Government of Northwest Territories) and Heather Scott (Mackenzie Valley Land and Water Board) for their assistance and feedback. We also thank Dr. Julia Guimond (Dalhousie University) for assistance with running simulations. This work was funded by the Government of the Northwest Territories, and the Natural Sciences and Engineering Research Council of Canada through a NSERC Discovery grant. This research was conducted while A. Mohammed held a fellowship through the Ocean Frontier Institute, an award from the Canada First Research Excellence Fund. An earlier version of the manuscript greatly benefited from reviews of Dr. Ethan Coon and 2 anonymous reviewers.

## References

- Albers, B. M. C., Molson, J. W., & Bense, V. F. (2020). Parameter sensitivity analysis of a two-dimensional cryo-hydrogeological numerical model of degrading permafrost near Umiujaq (Nunavik, Canada). *Hydrogeology Journal*, 28, 905–919. <https://doi.org/10.1007/s10040-020-02112-2>
- Al-Houri, Z. M., Barber, M. E., Yonge, D. R., Ullman, J. L., & Beutel, M. W. (2009). Impacts of frozen soils on the performance of infiltration treatment facilities. *Cold Regions Science and Technology*, 59(1), 51–57. <https://doi.org/10.1016/j.coldregions.2009.06.002>
- Barnes, D. L., & Chuvilin, E. (2009). Migration of petroleum in permafrost-affected regions. In *Permafrost soils* (pp. 263–278). Berlin, Heidelberg: Springer.
- Bear, J. (1972). *Dynamics of fluids in porous media*. Courier Corporation.
- Bense, V. F., Ferguson, G., & Kooi, H. (2009). Evolution of shallow groundwater flow systems in areas of degrading permafrost. *Geophysical Research Letters*, 36(22), L22401. <https://doi.org/10.1029/2009gl039225>
- Bense, V. F., Kooi, H., Ferguson, G., & Read, T. (2012). Permafrost degradation as a control on hydrogeological regime shifts in a warming climate. *Journal of Geophysical Research*, 117(F3), F03036. <https://doi.org/10.1029/2011jf002143>
- Biggar, K. W., Haidar, S., Nahir, M., & Jarrett, P. M. (1998). Site investigations of fuel spill migration into permafrost. *Journal of Cold Regions Engineering*, 12(2), 84–104. [https://doi.org/10.1061/\(asce\)0887-381x\(1998\)12:2\(84\)](https://doi.org/10.1061/(asce)0887-381x(1998)12:2(84))
- Bosson, E., Selroos, J. O., Stigsson, M., Gustafsson, L. G., & Destouni, G. (2013). Exchange and pathways of deep and shallow groundwater in different climate and permafrost conditions using the Forsmark site, Sweden, as an example catchment. *Hydrogeology Journal*, 21(1), 225–237. <https://doi.org/10.1007/s10040-012-0906-7>
- Burkow, I. C., & Kallenborn, R. (2000). Sources and transport of persistent pollutants to the Arctic. *Toxicology letters*, 112, 87–92. [https://doi.org/10.1016/s0378-4274\(99\)00254-4](https://doi.org/10.1016/s0378-4274(99)00254-4)
- Carlson, A. E., & Barnes, D. L. (2011). Movement of trichloroethene in a discontinuous permafrost zone. *Journal of Contaminant Hydrology*, 124(1–4), 1–13. <https://doi.org/10.1016/j.jconhyd.2010.11.002>
- Cary, J. W., & Mayland, H. F. (1972). Salt and water movement in unsaturated frozen soil. *Soil Science Society of America Journal*, 36(4), 549–555. <https://doi.org/10.2136/sssaj1972.03615995003600040019x>
- Collins, M., Knutti, R., Arblaster, J., Dufresne, J.-L., Fichet, T., Friedlingstein, P., et al. (2013). Long-term climate change: Projections, commitments and irreversibility. In T. F. Stocker, et al. (Eds.), *Climate change 2013 the physical science basis: Working group I contribution to the fifth assessment report of the intergovernmental panel on climate change* (Vol. 9781107057, pp. 1029–1136). Cambridge University Press.
- Connolly, C. T., Cardenas, M. B., Burkart, G. A., Spencer, R. G., & McClelland, J. W. (2020). Groundwater as a major source of dissolved organic matter to Arctic coastal waters. *Nature Communications*, 11(1), 1–8. <https://doi.org/10.1038/s41467-020-15250-8>



- Cvetkovic, V., Carstens, C., Selroos, J. O., & Destouni, G. (2012). Water and solute transport along hydrological pathways. *Water Resources Research*, 48(6), W06537. <https://doi.org/10.1029/2011wr011367>
- Dagenais, S., Molson, J., Lemieux, J.-M., Fortier, R., & Therrien, R. (2020). Coupled cryo-hydrogeological modelling of permafrost dynamics near Umiujaq (Nunavik, Canada). *Hydrogeology Journal*, 28, 887–904. <https://doi.org/10.1007/s10040-020-02111-3>
- Daley, K., Jamieson, R. C., Rainham, D., & Hansen, L. T. (2018). Wastewater treatment and public health in Nunavut: A microbial risk assessment framework for the Canadian Arctic. *Environmental Science and Pollution Research*, 25(33), 32860–32872. <https://doi.org/10.1007/s11356-017-8566-8>
- Diersch, H. J. G. (2013). *FEFLOW: Finite element modeling of flow, mass and heat transport in porous and fractured media*. Springer Science & Business Media.
- Ding, B., Rezaeezad, F., Gharedaghloo, B., Van Cappellen, P., & Passet, E. (2019). Bioretention cells under cold climate conditions: Effects of freezing and thawing on water infiltration, soil structure, and nutrient removal. *The Science of the Total Environment*, 649, 749–759. <https://doi.org/10.1016/j.scitotenv.2018.08.366>
- Dusek, J., Dohnal, M., Vogel, T., Marx, A., & Barth, J. A. (2019). Modelling multiseasonal preferential transport of dissolved organic carbon in a shallow forest soil: Equilibrium versus kinetic sorption. *Hydrological Processes*, 33(22), 2898–2917. <https://doi.org/10.1002/hyp.13536>
- Dyke, L. D. (2001). Contaminant migration through the permafrost active layer, Mackenzie Delta area, Northwest Territories, Canada. *Polar Record*, 37(202), 215–228. <https://doi.org/10.1017/s0032247400027248>
- Evans, S. G., & Ge, S. (2017). Contrasting hydrogeologic responses to warming in permafrost and seasonally frozen ground hillslopes. *Geophysical Research Letters*, 44(4), 1803–1813. <https://doi.org/10.1002/2016gl072009>
- Evans, S. G., Godsey, S. E., Rushlow, C. R., & Voss, C. (2020). Water tracks enhance water flow above permafrost in upland Arctic Alaska hillslopes. *Journal of Geophysical Research: Earth Surface*, 125(2), e2019JF005256. <https://doi.org/10.1029/2019jf005256>
- Fan, Z., Neff, J. C., & Wickland, K. P. (2010). Modeling the production, decomposition, and transport of dissolved organic carbon in boreal soils. *Soil Science*, 175(5), 223–232. <https://doi.org/10.1097/ss.0b013e3181e0559a>
- Flerchinger, G. N., & Saxton, K. E. (1989). Simultaneous heat and water model of a freezing snow-residue-soil system I. Theory and development. *Transactions of the American Society of Agricultural Engineers*, 32(2), 565–571. <https://doi.org/10.13031/2013.31040>
- Frampton, A., & Destouni, G. (2015). Impact of degrading permafrost on subsurface solute transport pathways and travel times. *Water Resources Research*, 51(9), 7680–7701. <https://doi.org/10.1002/2014WR016689>
- Frampton, A., Painter, S. L., & Destouni, G. (2013). Permafrost degradation and subsurface-flow changes caused by surface warming trends. *Hydrogeology Journal*, 21(1), 271–280. <https://doi.org/10.1007/s10040-012-0938-z>
- Ge, S., McKenzie, J., Voss, C., & Wu, Q. (2011). Exchange of groundwater and surface-water mediated by permafrost response to seasonal and long term air temperature variation. *Geophysical Research Letters*, 38(14), L14402. <https://doi.org/10.1029/2011gl047911>
- Ginot, F., Lenavetier, T., Dedovets, D., & Deville, S. (2020). Solute strongly impacts freezing under confinement. *Applied Physics Letters*, 116(25), 253701. <https://doi.org/10.1063/5.0008925>
- Government of Canada (2019). *Canadian climate normals 1981–2010 station data*. Retrieved from [https://climate.weather.gc.ca/climate\\_normals](https://climate.weather.gc.ca/climate_normals)
- Grenier, C., Anbergen, H., Bense, V., Chanzy, Q., Coon, E., Collier, N., et al. (2018). Groundwater flow and heat transport for systems undergoing freeze-thaw: Intercomparison of numerical simulators for 2D test cases. *Advances in Water Resources*, 114, 196–218. <https://doi.org/10.1016/j.advwatres.2018.02.001>
- Hayashi, M., Goeller, N., Quinton, W. L., & Wright, N. (2007). A simple heat-conduction method for simulating the frost-table depth in hydrological models. *Hydrological Processes*, 21(19), 2610–2622. <https://doi.org/10.1002/hyp.6792>
- Hayward, J. L., Jackson, A. J., Yost, C. K., Hansen, L. T., & Jamieson, R. C. (2018). Fate of antibiotic resistance genes in two Arctic tundra wetlands impacted by municipal wastewater. *The Science of the Total Environment*, 642, 1415–1428. <https://doi.org/10.1016/j.scitotenv.2018.06.083>
- Heginbottom, J. A., & Radburn, L. K. (1992). *Permafrost and ground ice conditions of northwestern Canada: Compiled by JA Heginbottom and LK Radburn, 1987*. Geological Survey of Canada.
- Hinzman, L. D., Goering, D. J., & Kane, D. L. (1998). A distributed thermal model for calculating soil temperature profiles and depth of thaw in permafrost regions. *Journal of Geophysical Research*, 103(D22), 28975–28991. <https://doi.org/10.1029/98jd01731>
- Jafarov, E. E., Coon, E. T., Harp, D. R., Wilson, C. J., Painter, S. L., Atchley, A. L., & Romanovsky, V. E. (2018). Modeling the role of preferential snow accumulation in through talik development and hillslope groundwater flow in a transitional permafrost landscape. *Environmental Research Letters*, 13(10), 105006. <https://doi.org/10.1088/1748-9326/aadd30>
- Jan, A., Coon, E. T., & Painter, S. L. (2020). Evaluating integrated surface/subsurface permafrost thermal hydrology models in ATS (v0.88) against observations from a polygonal tundra site. *Geoscientific Model Development*, 13(5), 2259–2276. <https://doi.org/10.5440/1545603>
- Johansson, E., Gustafsson, L. G., Berglund, S., Lindborg, T., Selroos, J. O., Liljedahl, L. C., & Destouni, G. (2015). Data evaluation and numerical modeling of hydrological interactions between active layer, lake and talik in a permafrost catchment, Western Greenland. *Journal of Hydrology*, 527, 688–703. <https://doi.org/10.1016/j.jhydrol.2015.05.026>
- Karra, S., Painter, S. L., & Lichtner, P. C. (2014). Three-phase numerical model for subsurface hydrology in permafrost-affected regions (PFLOTTRAN-ICE v1.0). *The Cryosphere*, 8(5), 1935–1950. <https://doi.org/10.5194/tc-8-1935-2014>
- Koch, J. C., Ewing, S. A., Striegl, R., & McKnight, D. M. (2013). Rapid runoff via shallow throughflow and deeper preferential flow in a boreal catchment underlain by frozen silt (Alaska, USA). *Hydrogeology Journal*, 21(1), 93–106. <https://doi.org/10.1007/s10040-012-0934-3>
- Krumhansl, K. A., Krkosek, W. H., Greenwood, M., Ragush, C., Schmidt, J., Grant, J., et al. (2015). Assessment of Arctic community wastewater impacts on marine benthic invertebrates. *Environmental Science & Technology*, 49(2), 760–766. <https://doi.org/10.1021/es503330n>
- Kurylyk, B. L., Hayashi, M., Quinton, W. L., McKenzie, J. M., & Voss, C. I. (2016). Influence of vertical and lateral heat transfer on permafrost thaw, peatland landscape transition, and groundwater flow. *Water Resources Research*, 52(2), 1286–1305. <https://doi.org/10.1002/2015wr018057>
- Lamontagne-Hallé, P., McKenzie, J. M., Kurylyk, B. L., Molson, J., & Lyon, L. N. (2020). Guidelines for cold-regions groundwater numerical modeling. *WIREs Water*, 7(6), e1467. <https://doi.org/10.1002/wat2.1467>
- Lamontagne-Hallé, P., McKenzie, J. M., Kurylyk, B. L., & Zipper, S. C. (2018). Changing groundwater discharge dynamics in permafrost regions. *Environmental Research Letters*, 13(8), 084017. <https://doi.org/10.1088/1748-9326/aad404>
- Langford, J. E., Schincariol, R. A., Nagare, R. M., Quinton, W. L., & Mohammed, A. A. (2020). Transient and transition factors in modeling permafrost thaw and groundwater flow. *Groundwater*, 58(2), 258–268. <https://doi.org/10.1111/gwat.12903>
- Lunardini, V. J. (1988). *Freezing of soil with an unfrozen water content and variable thermal properties*. U.S. Army Corps of Engineers Cold Regions Research and Engineering Laboratory.



- Macdonald, R. W., Barrie, L. A., Bidleman, T. F., Diamond, M. L., Gregor, D. J., Semkin, R. G., & Alexeeva, L. B. (2000). Contaminants in the Canadian Arctic: 5 years of progress in understanding sources, occurrence and pathways. *The Science of the Total Environment*, 254(2–3), 93–234. [https://doi.org/10.1016/S0048-9697\(00\)00434-4](https://doi.org/10.1016/S0048-9697(00)00434-4)
- Macdonald, R. W., Harner, T., & Fyfe, J. (2005). Recent climate change in the Arctic and its impact on contaminant pathways and interpretation of temporal trend data. *The Science of the Total Environment*, 342(1–3), 5–86. <https://doi.org/10.1016/j.scitotenv.2004.12.059>
- Malmström, M. E., Destouni, G., & Martinet, P. (2004). Modeling expected solute concentration in randomly heterogeneous flow systems with multicomponent reactions. *Environmental Science & Technology*, 38(9), 2673–2679. <https://doi.org/10.1021/es030029d>
- McCarter, C. P. R., Branfireun, B. A., & Price, J. S. (2017). Nutrient and mercury transport in a sub-arctic ladder fen peatland subjected to simulated wastewater discharges. *The Science of the Total Environment*, 609, 1349–1360. <https://doi.org/10.1016/j.scitotenv.2017.07.225>
- McCray, J. E., Kirkland, S. L., Siegrist, R. L., & Thyne, G. D. (2005). Model parameters for simulating fate and transport of on-site wastewater nutrients. *Groundwater*, 43(4), 628–639. <https://doi.org/10.1111/j.1745-6584.2005.00777.x>
- McKenzie, J. M., Kurylyk, B. L., Walvoord, M. A., Bense, V. F., Fortier, D., Spence, C., & Grenier, C. (2021). Invited perspective: What lies beneath a changing Arctic? *The Cryosphere*, 15(1), 479–484. <https://doi.org/10.5194/tc-15-479-2021>
- McKenzie, J. M., Voss, C. I., & Siegel, D. I. (2007). Groundwater flow with energy transport and water–ice phase change: Numerical simulations, benchmarks, and application to freezing in peat bogs. *Advances in Water Resources*, 30(4), 966–983. <https://doi.org/10.1016/j.advwatres.2006.08.008>
- Mohammed, A. A., Cey, E. E., Hayashi, M., Callaghan, M. V., Park, Y.-J., Miller, K. L., & Frey, S. K. (2021). Dual-permeability modeling of preferential flow and snowmelt partitioning in frozen soils. *Vadose Zone Journal*, 20, e20101. <https://doi.org/10.1002/vzj2.20101>
- Mohammed, A. A., Schincariol, R. A., Quinton, W. L., Nagare, R. M., & Flerchinger, G. N. (2017). On the use of mulching to mitigate permafrost thaw due to linear disturbances in sub-arctic peatlands. *Ecological Engineering*, 102, 207–223. <https://doi.org/10.1016/j.ecoleng.2017.02.020>
- Neilson, B. T., Cardenas, M. B., O'Connor, M. T., Rasmussen, M. T., King, T. V., & Kling, G. W. (2018). Groundwater flow and exchange across the land surface explain carbon export patterns in continuous permafrost watersheds. *Geophysical Research Letters*, 45(15), 7596–7605. <https://doi.org/10.1029/2018gl078140>
- Ogata, A., & Banks, R. B. (1961). *A solution of the differential equation of longitudinal dispersion in porous media*. US Geological Survey Report, paper 411-A. <https://doi.org/10.3133/pp411a>
- Orgogozo, L., Prokushkin, A. S., Pokrovsky, O. S., Grenier, C., Quintard, M., Viers, J., & Audry, S. (2019). Water and energy transfer modeling in a permafrost-dominated, forested catchment of Central Siberia: The key role of rooting depth. *Permafrost and Periglacial Processes*, 30(2), 75–89. <https://doi.org/10.1002/ppp.1995>
- Painter, S. L., Coon, E. T., Atchley, A. L., Berndt, M., Garimella, R., Moulton, J. D., & Svyatskiy, C. J. (2016). Integrated surface/subsurface permafrost thermal hydrology: Model formulation and proof-of-concept simulations. *Water Resources Research*, 52(8), 6062–6077. <https://doi.org/10.1002/2015wr018427>
- Panday, S., & Corapcioglu, M. Y. (1994). Theory of phase-separate multicomponent contaminant transport in frozen soils. *Journal of Contaminant Hydrology*, 16(3), 235–269. [https://doi.org/10.1016/0169-7722\(94\)90038-8](https://doi.org/10.1016/0169-7722(94)90038-8)
- PDE Solutions Inc. (2020). *FlexPDE manual version 7.16*. Spokane Valley, WA, USA.
- Poland, J. S., Riddle, M. J., & Zeeb, B. A. (2003). Contaminants in the Arctic and the Antarctic: A comparison of sources, impacts, and remediation options. *Polar Record*, 39(4), 369–383. <https://doi.org/10.1017/S0032247403002985>
- Schincariol, R. A., Schwartz, F. W., & Mendoza, C. A. (1997). Instabilities in variable density flows: Stability and sensitivity analyses for homogeneous and heterogeneous media. *Water Resources Research*, 33(1), 31–41. <https://doi.org/10.1029/96wr02587>
- Selroos, J. O., Cheng, H., Vidstrand, P., & Destouni, G. (2019). Permafrost thaw with thermokarst wetland-lake and societal-health risks: Dependence on local soil conditions under large-scale warming. *Water*, 11(3), 574. <https://doi.org/10.3390/w11030574>
- Sjöberg, Y., Coon, E., Sannel, K. A. B., Pannetier, R., Harp, D., et al. (2016). Thermal effects of groundwater flow through subarctic fens: A case study based on field observations and numerical modeling. *Water Resources Research*, 52(3), 1591–1606. <https://doi.org/10.1002/2015wr017571>
- Smith, S. L., Wolfe, S. A., Riseborough, D. W., & Nixon, F. M. (2009). Active-layer characteristics and summer climatic indices, Mackenzie Valley, Northwest Territories, Canada. *Permafrost and Periglacial Processes*, 20(2), 201–220. <https://doi.org/10.1002/ppp.651>
- Trinchero, P., Painter, S. L., Poter, A., Sanglas, J., Cvetkovic, V., & Selroos, J. O. (2020). A particle-based conditional sampling scheme for the simulation of transport in fractured rock with diffusion into stagnant water and rock matrix. *Water Resources Research*, 56(4), e2019WR026958. <https://doi.org/10.1029/2019wr026958>
- Vonk, J. E., Tank, S. E., & Walvoord, M. A. (2019). Integrating hydrology and biogeochemistry across frozen landscapes. *Nature Communications*, 10(1), 1–4. <https://doi.org/10.1038/s41467-019-13361-5>
- Walvoord, M. A., Voss, C. I., & Wellman, T. P. (2012). Influence of permafrost distribution on groundwater flow in the context of climate-driven permafrost thaw: Example from Yukon Flats Basin, Alaska, United States. *Water Resources Research*, 48(7), W07524. <https://doi.org/10.1029/2011wr011595>
- Wittgren, H. B., & Mrethlum, T. (1997). Wastewater treatment wetlands in cold climates. *Water Science and Technology*, 35(5), 45–53. <https://doi.org/10.2166/wst.1997.0162>
- Yi, X., Su, D., Bussière, B., & Mayer, K. U. (2021). Thermal-hydrological-chemical modeling of a covered waste rock pile in a permafrost region. *Minerals*, 11(6), 565. <https://doi.org/10.3390/min11060565>
- Yurova, A., Sirin, A., Buffam, I., Bishop, K., & Laudon, H. (2008). Modeling the dissolved organic carbon output from a boreal mire using the convection-dispersion equation: Importance of representing sorption. *Water Resources Research*, 44(7), W07411. <https://doi.org/10.1029/2007wr006523>
- Zhou, J., Meng, X., Wei, C., & Pei, W. (2020). Unified soil freezing characteristic for variably-saturated saline soils. *Water Resources Research*, 56(7), e2019WR026648. <https://doi.org/10.1029/2019wr026648>

## References From the Supporting Information

- Campbell, G. S. (1974). A simple method for determining unsaturated conductivity from moisture retention data. *Soil Science*, 117(6), 311–314. <https://doi.org/10.1097/00010694-197406000-00001>
- Flerchinger, G. N. (2000). *The simultaneous heat and water (SHAW) model: Technical documentation*. Northwest Watershed Research Center, USDA Agricultural Research Service.

- Flerchinger, G. N., Seyfried, S. M., & Hardegee, S. P. (2006). Using soil freezing characteristics to model multi-season soil water dynamics. *Vadose Zone Journal*, 5(4), 1143–1153. <https://doi.org/10.2136/vzj2006.0025>
- Fuchs, M., Campbell, G. S., & Papendick, R. I. (1978). An analysis of sensible and latent heat flow in a partially frozen unsaturated soil. *Soil Science Society of America Journal*, 42(3), 379–385. <https://doi.org/10.2136/sssaj1978.03615995004200030001x>
- Smith, M. W., & Riseborough, D. W. (2002). Climate and the limits of permafrost: A zonal analysis. *Permafrost and Periglacial Processes*, 13(1), 1–15. <https://doi.org/10.1002/ppp.410>
- Zhang, Y., Chen, W., Smith, S. L., Riseborough, D. W., & Cihlar, J. (2005). Soil temperature in Canada during the twentieth century: Complex responses to atmospheric climate change. *Journal of Geophysical Research*, 110(D3), D03112. <https://doi.org/10.1029/2004jd004910>